Experiments in Fluids (2022) 63:45
https://doi.org/10.1007/s00348-022-03380-2

RESEARCH ARTICLE

# Flow–acoustic coupling around rectangular rods of different aspect ratios and incidence angles

**Mahmoud Shaaban**[1] · **Atef Mohany**[1]

Received: 21 May 2021 / Revised: 2 January 2022 / Accepted: 4 January 2022
© The Author(s), under exclusive licence to Springer-Verlag GmbH Germany, part of Springer Nature 2022

## Abstract

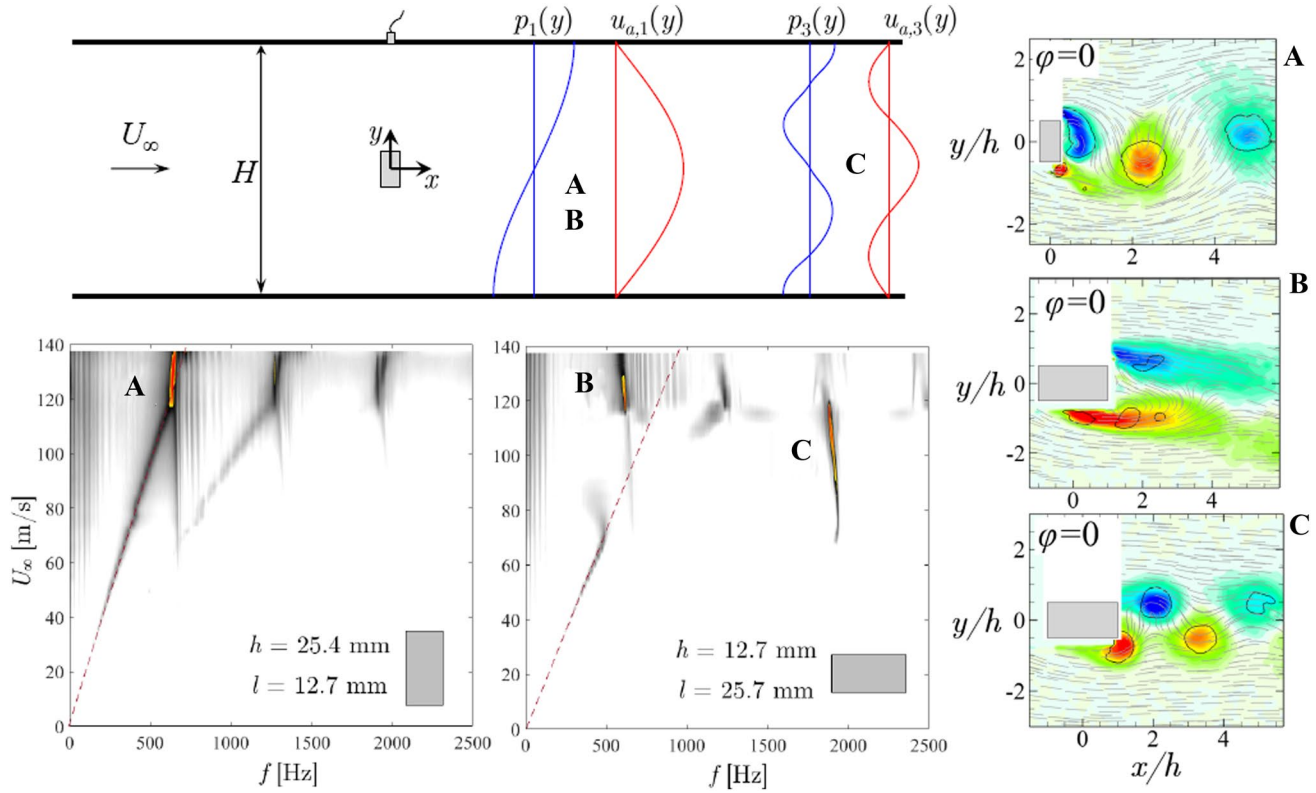
The excitation of the transverse acoustic modes of a duct by the flow around rectangular rods with sharp corners is experimentally investigated. Emphasis is given to the unique role of the rod's flow incidence angle and its cross section aspect ratio on the flow structure and its susceptibility to resonance excitation. Two different mechanisms that lead to acoustic resonance excitation are identified. The first mechanism is triggered by the vortex shedding observed downstream of the square rod regardless of its aspect ratio. The second mechanism is triggered by the interaction of the separated shear layers from the rod's upstream corners with the rod's trailing edges, and it results in an abrupt excitation of the third acoustic cross-mode at conditions that depend on the side length of the rod. Moreover, the excitation of this mechanism occurs at lower flow velocities than those required to excite the first acoustic mode, which is not the case for circular cylinders in cross-flow. The Strouhal number and the symmetry of the vortex shedding from the square rod have profound dependence on the rod's aspect ratio and its flow incidence angle, which, in turn, affect the amplitude of the excited acoustic pressure and the lock-in velocity range. Asymmetric vortex shedding can alleviate the intensity of acoustic resonance, where the minimum acoustic pressure occurs close to an incidence angle of 9°. However, this reduction should be carefully considered as rods at low flow incidence angles may excite resonance of higher-order acoustic cross-modes at lower flow velocities over a wider lock-in range.

✉ Mahmoud Shaaban
mahmoud.shaaban@ontariotechu.net

[1] Aeroacoustics and Noise Control Laboratory, University of Ontario Institute of Technology, Oshawa, ON, Canada

Published online: 15 February 2022

**Graphical abstract**




**List of symbols**

| | |
|---|---|
| $U_\infty$ | Inlet flow velocity |
| $U_{res}$ | Inlet flow velocity at peak of resonance |
| $St$ | Strouhal number |
| $f$ | Frequency |
| $f_a$ | Acoustic mode frequency |
| $x$, $y$ | Streamwise, crosswise coordinates |
| $p$ | Acoustic pressure |
| $v_{a,n}$ | Acoustic particle velocity of the $n^{th}$ mode |
| $h$ | Rectangular cross section height |
| $l$ | Rectangular cross section side length |
| $\alpha$ | Flow incidence angle |
| $d$ | Blockage length |
| $w$ | max($h$, $l$) |
| $k$ | Wave number |
| $n$ | Acoustic cross-mode number |
| $c$ | Speed of sound in air |
| $\varphi$ | Acoustic pressure phase angle |
| $\Delta U$ | Lock-in flow velocity range |
| $\rho$ | Flow density |
| $\omega_z$ | Vorticity in the $x$-$y$ plane |
| $Re$ | Reynolds number |
| $M$ | Mach number |
| $H$ | Test section height |
| $B$ | Test section width |

## 1 Introduction

Severe noise and vibration induced by flow–acoustic coupling have been reported as a design challenge in many engineering applications that include periodic flow instabilities, such as jet flow (Mancinelli et al. 2019), cavity flow (Léon et al. 2019), wind turbines (Pereira et al. 2020), side branches (Dequand et al. 2003; Tonon et al. 2011), cylinder arrangements (Mohany and Ziada 2005), turbomachines (Clark et al. 2015; Tian et al. 2018; Fiquet et al. 2020), and several other applications (Ziada 2010). During acoustic resonance excitation, a significant generation of acoustic energy can be sustained when periodic flow instabilities couple with an acoustic mode. This leads to acute noise that is often associated with excessive vibration which could result in operation interruption and in some cases may escalate rapidly to catastrophic failures (NRC 2004). Self-excitation of acoustic resonance has received considerable attention over the past decade

due to the strict safety regulations and the ever-increasing demand for capacity and reliability of impacted equipment.

Blevins and Bressler (1993) experimentally identified vortex shedding in the wake of a single circular cylinder as the excitation source of transverse acoustic modes in a duct. The velocity and pressure perturbations induced by vortex shedding occur at a frequency that is dependent on the flow velocity. Moreover, sound generation by vortex shedding induces a dipole sound source in the direction of the fluctuating lift force (Inoue and Hatakeyama 2002). The acoustic mode frequencies of the surrounding duct can coincide with the vortex shedding frequency at certain flow velocities. If the dipole source is oriented in the direction of the acoustic particle velocity, the acoustic oscillations can grow stronger driven by the flow fluctuation, which in turn "locks-in" to the frequency of the acoustic mode and results in a resonant acoustic field (Keller and Escudier 1983). The excited acoustic mode resonates and the acoustic particle velocity may reach amplitudes up to 10% of the mean flow velocity, enhancing the flow vorticity and increasing the correlation length along the span of the cylinder, which is bound to increase the amplitude of the dynamic lift force (Blevins 1985). Acoustic oscillations can organize the vortex shedding pattern and enhances the uniformity and the two-dimensionality of vortex shedding (Islam et al. 2020). Mohany and Ziada (2011) have experimentally quantified the increase in the dynamic lift force acting on a circular cylinder due to the excitation of acoustic resonance. They reported an increase in the dynamic lift coefficient by a factor of 4 compared to that observed before the onset of acoustic resonance.

Flow-excited acoustic resonance has been reported in several configurations, such as a single cylinder (Blevins 1984), tandem cylinders (Mohany and Ziada 2005), closely packed arrays (Ziada et al. 1989), deep cavities (Ziada and Shine 1999), and side branches (Uchiyama and Morita 2017) with different excitation mechanisms in play. Ziada et al. (1989) reported that closely packed arrays of cylinders are capable of exciting acoustic resonance due to some but not all of the flow instabilities present in the cylinder wakes. For a single cylinder in a cross-flow, the mechanism of resonance excitation was attributed only to the vortex shedding downstream of the cylinder (Blevins and Bressler 1993). Mohany and Ziada (2005) showed that flow around circular cylinders in tandem can excite acoustic resonance due to coupling with two distinguished flow patterns. First, vortex shedding in the wake excites acoustic resonance at frequency coincidence, with characteristics that depend on the configuration of the cylinder arrangement. Second, resonance may occur at flow velocities lower than necessary for frequency coincidence between vortex shedding and the acoustic mode. This behavior was attributed to the separation and impingement of the shear layer over the gap between the two cylinders. Shaaban and Mohany (2020) showed that flow over inline cylinders can excite resonance by similar mechanisms, where complex interaction of the gap flow leads to significant changes in the strength and spectral characteristics of the resulting acoustic resonance. Despite the extensive work that exists in the literature about the coupling between the flow around circular cylinders in different arrangements with resonant acoustic modes, up to the authors' knowledge, no similar attempts were made for the case of square cylinders in cross-flow.

The instabilities arising from the flow coupling with structural and acoustic modes are of great practical concern as they may lead to undesired noise, vibration, fatigue damage of structures, or even structural failures. When exposed to fluid flow, the vibration and aerodynamic features of the sharp-edged square cross sections are well documented (Knisely 1990). When a rod of a square cross section is placed in cross-flow, a complex pattern of flow features is observed, characterized by a large region of flow separation with suction pressure, resulting in significant mean and dynamic forces (Zhang et al. 2005). The aerodynamic features of a square rod in cross-flow are sensitive to the cross section aspect ratio and the flow incidence angle (Van Oudheusden et al. 2005). Okajima (1982) observed that the Strouhal number for periodic vortex shedding downstream of a single square rod at a zero angle of attack has no significant dependence on Reynolds numbers higher than $10^3$. Dobre and Hangan (2004) used a hot-wire anemometer to study the wake topology of a square rod for high Reynolds number and reported that the flow structures in the wake of a square rod share characteristics of the wakes of indented flat plates and circular cylinders. Knisely (1990) experimentally determined Strouhal numbers for rectangular rods of different cross section aspect ratios at varying angles of attack, reporting a rapid rise in the Strouhal number at relatively small angles of attack associated with reattachment of the separated shear layer. Yen and Yang (2011) investigated the effect of Reynolds number and incidence angle on the wake flow characteristics of a square rod. They reported that the flow structures in the wake exhibit three modes: leading-edge separation, separation bubble, and attached flow, as determined from the flow topology. The incidence angle had a significant effect on the fluctuating forces as well as the Strouhal number of vortex shedding in the wake Dutta et al. (2003). In contrast with circular cylinders, van Hinsberg (2021) reported that the separation points on rods square cross sections are independent of Reynolds number and surface roughness. Norberg (1993) showed that multiple oscillation frequencies exist in the wake at low incidence angle with a dependency on the blockage projected width. More recently, Margnat (2015) numerically investigated the generation of sound by vortex shedding downstream of a rectangular rod at various incidence angles and low Reynolds numbers. They showed that the efficiency of the sound

generation is closely linked to the wake organization, the location of the stagnation point, and the orientation of the fluctuating aerodynamic force. Moreover, they showed that the efficiency of sound generation increases with the Mach number, the fluctuating lift and drag force amplitudes, and the Strouhal number. da Silva Pinto and Margnat (2020) investigated noise generation by cylinder with polygonal cross section and reported that the fluctuating lift is the major quantity to control noise at fixed length, while increasing the aspect ratio tends to reduce the noise for globally all geometries. Although the available work in the literature has improved our understanding of the flow structure and the sound radiation from square rods, the resonant coupling between the flow around square rods with transverse acoustic modes has never been investigated before.

The excitation mechanism of acoustic resonance by cross-flow over cylinders is closely related to vortex-induced vibration of bluff bodies (Sarpkaya 2004). Brooks (1960) investigated the vortex-induced vibration of a circular cylinder constrained to oscillate transversely in a free stream and reported that the axial symmetry restricts the mechanism of vibration to a single mechanism at each Reynolds number. Measurements of vortex-induced vibration of a single circular cylinder identified the Strouhal number and the fluctuating lift in steady flow about a cylinder at rest as the controlling parameter of the coupled cylinder motion (Norberg 2003). On the other hand, structures with axial asymmetry such as a rod with a square cross section may be susceptible to other flow-induced mechanisms such as transverse galloping (Rockwell 1977). Bearman et al. (1987) experimentally investigated the galloping instability of a square cylinder and reported a strong third-harmonic frequency of the body oscillation in the transverse lift frequency components at a certain flow velocity. However, no attempts were made to investigate the potential for the many involved parameters on the self-excitation of acoustic resonance by the dynamic wake flow of rectangular rods.

The dynamic features of the flow around rods of rectangular cross sections indicate that such structures are susceptible to fluid-resonant mechanisms which may lead to resonance self-excitation. However, the presence of potential lock-in Strouhal numbers and the characteristics of flow–acoustic coupling that may lead to severe acoustic resonance are not reported in the literature. Although structures of rectangular cross sections are vital for various applications with a confined cross-flow, the aeroacoustic response of this simple configuration is not yet available, and the nature of the potential interaction between the acoustic mode and the dynamic flow in the wake is not understood. Such knowledge is sought to safeguard designs against the possibility of a potentially damaging excitation of acoustic resonance at certain flow velocities. Therefore, this experimental work investigates the aeroacoustic response of a single rod with a rectangular cross section confined in a rectangular duct and subjected to a cross-flow. The effect of the aspect ratio and flow incidence angle is experimentally determined. The acoustic pressure development with the flow velocity, as well as the lock-in Strouhal numbers for dominant modes, is presented. Phase-locked particle image velocimetry is used to identify the flow topology coupled to acoustic resonance in the presence of a strong acoustic oscillation. The discussion in this study provides a basis to model the flow–acoustic coupling and predict the flow velocity at which acoustic resonance can occur for rectangular rod configurations.

## 2 Methodology

Experimental measurements were carried out in an open-loop wind tunnel. Air is drawn into the test section through a bell mouth by a centrifugal blower located at the downstream end of the wind tunnel. Figure 1 shows a simplified schematic of the test section configuration. The cross section of the test section is rectangular with a width $B = 127$ mm and a height $H = 254$ mm, and its length is sufficiently long in order to ensure uniform flow profiles and minimize acoustic radiation losses through the inlet and outlet boundaries. The subsequent diffuser section is connected to the air blower using a flexible duct connection to isolate vibration between the blower and the wind tunnel. Measurements of flow velocity profiles at the location of the rods showed that the turbulence intensity does not exceed 1% at the maximum achievable flow velocity inside the test section.

Inlet flow velocity is measured using a pitot tube, which is used to calibrate the wind tunnel air drive frequency, and

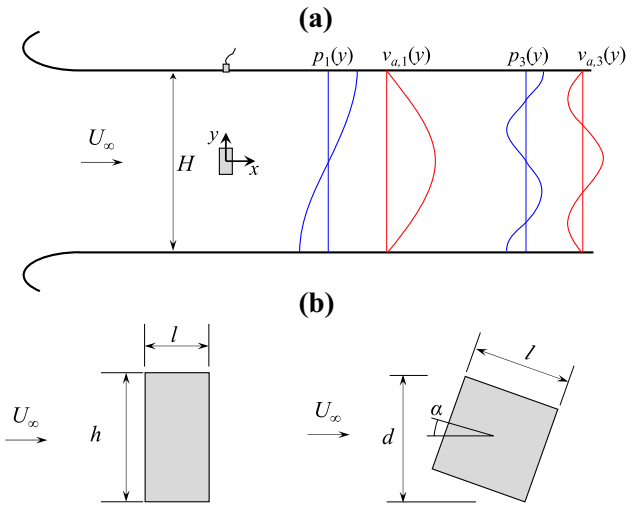



**Fig. 1** **a** A schematic of the experimental configuration and **b** a nomenclature of the cross section parameters.

is not used during self-excitation of acoustic resonance to avoid any interference with the flow and acoustic modes.

Rods of rectangular cross sections with different side lengths and aspect ratios are used. Lengths and heights between 9.5 mm and 25.4 mm, covering aspect ratios between $l/h = 0.375$ to 2.67, were investigated. The effect of flow incidence angle was investigated using blocks of square sections with two selected side lengths $l = 19.5$ mm and 25.4 mm, at incidence angles between 0 and 45°. Twenty-three rods were tested including five rods of a square cross section. The tested rod is attached horizontally from side to side in the middle of the test section height. The theoretical frequency of the first acoustic cross-mode in the wind tunnel can be calculated as $f_a = c/2H = 675$ Hz, and the third mode frequency is 2025 Hz, in agreement with the experimental observation.

To evaluate the aeroacoustic response for each case, the acoustic pressure is measured at a steady inlet flow velocity. The tested rod is subjected to flow velocities between 20 and 140 m/s, covering a range of $Re = 1.2 \times 10^4$ to $2.3 \times 10^5$ based on the cross section height. Acoustic pressure measurements are carried out using a 1/4 inch pressure microphone, flush-mounted to the top boundary of the test section at the anti-node of the acoustic pressure corresponding to the excited acoustic cross-modes. The microphone is attached exactly above the cylinder centerline. The pressure signal is recorded for a duration of 120 s at a sampling frequency of 20 kHz. The frequency spectrum is calculated using the Welch's modified periodogram method with 50% overlap and 1 Hz frequency resolution (Welch 1967). The inlet flow velocity is measured with a maximum error of ±2.2%, and the acoustic pressure is measured with an uncertainty of ±1.1%.

The dynamic characteristics of the wake flow downstream of selected rectangular configurations at incidence angle of 0° were investigated by means of phase-locked particle image velocimetry. A simplified description of the setup is shown in Figure 2. The $x - y$ wake plane at the midspan of the rod is illuminated by Nd:YAG laser beams with a wave length of 532 nm. The flow is seeded with particles of di-ethyl-hexyl-sebacate (DEHS) that have a maximum particle size of 1 $\mu$m. PIV measurements were carried out at a flow velocity that corresponds to the maximum acoustic pressure amplitudes during resonance excitation. The acoustic pressure signal was used to trigger the PIV system and initiate measurements of image pairs at a selected phase with respect to the acoustic pressure signal. To adjust the locked phase and cover a full acoustic pressure cycle, laser pulses were emitted at a selected time delay after the trigger by the acoustic pressure signal. For each phase, 250 instantaneous images were acquired as a set. Eight sets of measurements were taken at eight uniformly spaced phases of the acoustic cycle. The time between the laser pulses was adjusted to capture the maximum particle displacement

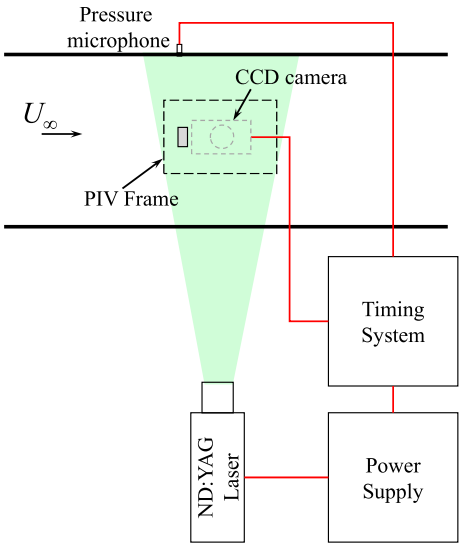



**Fig. 2** Particle image velocimetry setup used for phase-locked measurements

within one-quarter of the final interrogation window used for vector calculation, which are performed using a multi-pass cross-correlation algorithm with one pass at initial window size of $64 \times 64$ pixel$^2$ with 50% overlap and four final passes at interrogation window size of $32 \times 32$ pixel$^2$ with 50% overlap. The uncertainty in the flow quantities is evaluated using the correlation statistics method (Sciacchitano and Wieneke 2016). The final vector field has a uniform spatial resolution of $1.5 \times 1.5$ mm$^2$ with a maximum uncertainty of ±3.1 m/s, equivalent to less than 4.0% of the incoming flow velocity $U_\infty$. The vorticity $\omega_z$ is calculated using a second-order least-squares differential scheme with a maximum uncertainty of 7%.

## 3 Effect of cross section aspect ratio on acoustic resonance excitation

The aeroacoustic response of the rod showed significant dependency on its aspect ratio and cross section size. Figure 3 presents the characteristics of the pressure signal for four selected rod configurations at a range of flow velocities, shown in the frequency domain. Results are shown for two square cross section cases with two edge lengths $l = 19.1$ mm and $l = 25.4$ mm, and two rectangular cross section cases with aspect ratios of $l/h = 0.5$ and 2.0. For all cases, the pressure signal at low flow velocities up to 80 m/s was dominated by a tonal frequency peak that depends linearly on the flow velocity according to the constant Strouhal number relationship:

$$\mathrm{St} = \frac{fh}{U_\infty} \tag{1}$$

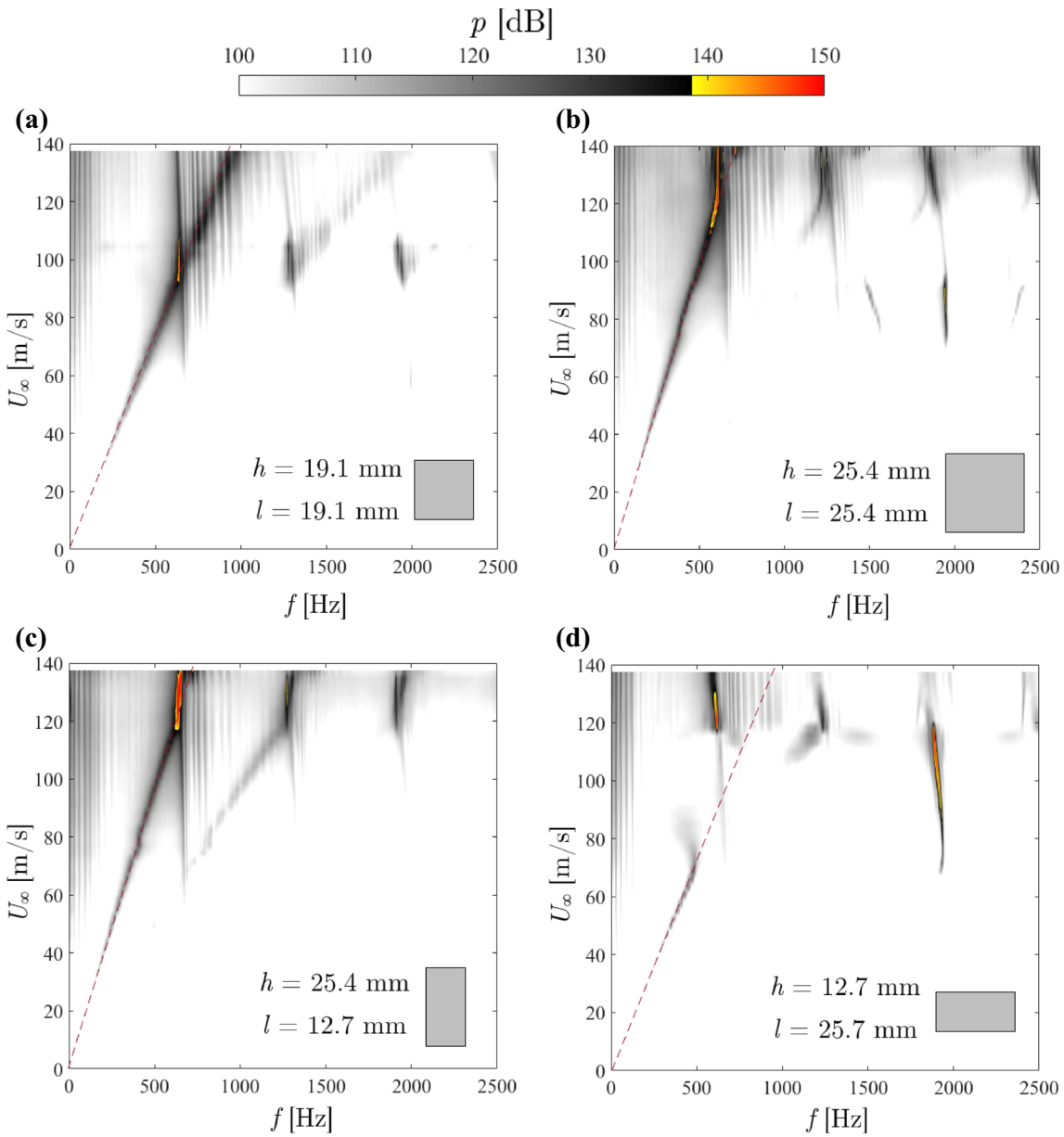



**Fig. 3** Spectral characteristics of the acoustic pressure for selected rectangular rods at different flow velocities

This peak has the typical features attributed to alternating vortex shedding from bluff bodies. The Strouhal number depends mainly on the rod dimensions. For cases in Fig. 3a and 3c, the frequency of the vortex shedding peak increases as the flow velocity increases, until it becomes in coincidence with the acoustic cross-mode frequency of the duct. At coincidence, the acoustic pressure increases significantly and tonal noise with pressure levels in excess of 145 dB indicates the excitation of sustained acoustic resonance. Under resonant conditions, the vortex shedding and the acoustic signal are locked-in to the same frequency over a range of flow velocities. As the flow velocity increases further, vortex shedding exits the lock-in condition and its frequency starts to increase further, and the acoustic pressure drops significantly.

An additional feature is observed for the configurations in Fig. 3b and 3 d. At flow velocities lower than necessary to excite the first acoustic mode, the excitation of the third acoustic cross-mode takes place, with frequencies close to 2000 Hz. This occurs prematurely at lower flow velocities that do not cause coincidence of vortex shedding with the first acoustic cross-mode frequency. This is quite surprising since the excitation of higher-order acoustic cross-modes usually requires higher flow energy. The excitation of the third acoustic cross-mode at low flow velocity was primarily dependent on the length of the rod cross section $l$ so that it

was observed only for rods with $l \geq 0.022$ m. For the same aspect ratio, the third mode may be excited for higher values of the length $l$. For example, cases 3a and 3 b in Fig. 3 have the same aspect ratio of 1.0, but the third mode was only excited for the configuration with the longer side length. The characteristics of this resonance are somehow similar to the pre-coincidence resonance reported for the configurations of tandem cylinders and inline cylinders, which were attributed to the flow structures in the gap between cylinders (Mohany and Ziada 2005; Shaaban and Mohany 2019b, a). However, the earlier excitation of acoustic resonance for these cases was reported for the first acoustic cross-mode and not for the higher acoustic modes. Moreover, the occurrence of similar flow structures around rods of rectangular cross sections is not possible. A common feature of these configurations is that the topology and instability in the wake is dependent on more than a single length scale. For tandem and inline cylinders, the gaps between cylinders allow for unstable flow different than vortex shedding, depending on the spacing and the diameter of the inline cylinders. Likewise, different flow regimes can exist around rectangular rods depending on the cross section height $h$ as well as the length $l$. The wake downstream of a rectangular rods is distinguished from that of circular cylinders by the separation and interaction on the sharp corners at the leading and trailing rod faces, as discussed in detail in the next section.

Figure 4 shows the Strouhal number associated with vortex shedding as detected in the acoustic pressure signal. For each case, the Strouhal number is determined over the same range of flow velocities without including the lock-in region. The figure shows that the Strouhal number responsible for the excitation of the coincidence resonance is in good agreement with the experimental results. The scatter of the Strouhal number values observed in the measurements at this range of $l/h$ is attributed to the effect of Reynolds numbers on the flow structure around the different rods, as the aeroacoustic effects are observed over significantly different ranges of flow velocities depending on the dimensions of $h$ and $l$ rather than the aspect ratio. For blunt rods of a low aspect ratio $l/h$, the Strouhal number $St_h$ starts at a stable value approaching 0.14 at very low values of $l$. At an aspect ratio $l/h = 1$, the Strouhal number is $St_h = 0.135$. Further increases in the aspect ratio result in a rapid decrease in the Strouhal numbers, reaching values of $St_h = 0.06$ at $l/h = 2.5$. The dependency of the Strouhal number on the rod cross section dimensions means that the excitation of acoustic resonance is expected at flow velocities that depend on both the height $h$ and the length $l$ of the rod. Fortunately, reliable values of the Strouhal number for vortex shedding from rectangular rods are available over a wide range of aspect ratios and Reynolds numbers (Bearman and Trueman 1972; Knisely 1990; Parker and Welsh 1983). These pieces of information can provide a reasonable estimate of the frequency at which acoustic resonance excitation may occur.

It is beneficial to inspect the dependency of the Strouhal number on the side dimensions of the rod to gain more insight of the flow features in the wake. Figure 5 presents the values of Strouhal number $St_w$, based on the larger side dimensions $w = \max(h, l)$. At aspect ratios lower than 1.0, the Strouhal number is based on the height $h$, and has a stable value around 0.135. The overwhelming dependency of the vortex shedding frequency on $h$ is a result of the separation at the two sharp corners on the leading face of the rod. As the rod length is small, the vortices do not interact with the trailing corners of the rod, and hence the length has no effect on the shedding frequency. On the other hand, the frequency of vortex shedding from slender rods with a high aspect ratio $l/h$ is dependent mainly on the length, as the separated shear layers interact with the trailing edge of the rod before rolling into vortices. At moderate aspect ratios between 1.0 and 1.5, a transition is observed. It is also likely that the interaction of the shear flow with the trailing edge plays an important role in the excitation of the third mode, as it is mainly observed for cross sections with a large side length $l$.

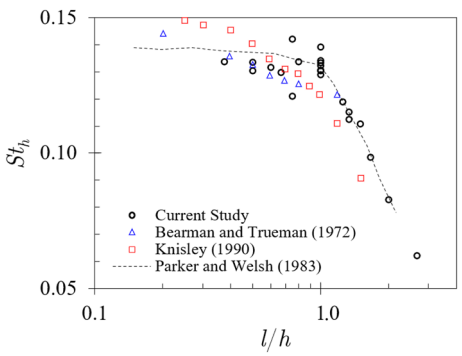



**Fig. 4** The Strouhal number of vortex shedding $St_h$ based on the cylinder height $h$ for rods with different aspect ratios

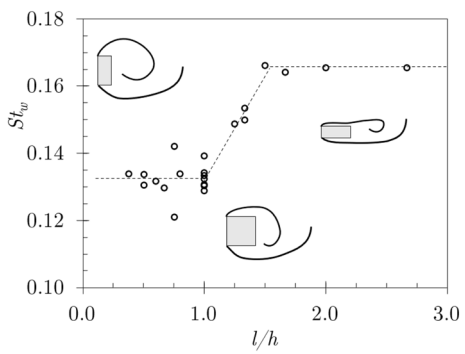



**Fig. 5** Strouhal numbers $St_w$ of vortex shedding based on the larger side dimensions $w$ at different rod aspect ratios

Figure 6 shows the acoustic pressure at the peak of acoustic resonance for all investigated configurations. The results suggest that the acoustic pressure can be well predicted by the square of the flow velocity at the conditions of resonance excitation. The scaling of the acoustic pressure with $\rho U^2$ is typical for excitation of acoustic resonance by separated flow over rectangular cavities (Rockwell and Naudascher 1978), which suggests that the common feature of flow separation at sharp edges may lead to related phenomena that excite acoustic resonance by similar mechanisms.

Figure 6 also shows that the excitation of the third acoustic cross-mode has a quadratic dependency on the flow velocity, with a lower proportionality constant. The lower acoustic pressure for third mode excitation at the same flow velocity indicates a higher loss of acoustic energy, which is excepted due to the significantly higher acoustic mode frequency. The excitation of the two acoustic modes shares the same minimum flow velocity at the condition of acoustic resonance. Results in Fig. 6 suggest that the acoustic resonance excitation is unlikely at flow velocities below $\sqrt{2.5 \times 10^3} = 50$ m/s. Lower flow velocities provide less available flow kinetic energy for the coupled flow–acoustic cycle. If the energy dissipation by mechanisms such as acoustic radiation and turbulence are significant compared to the excited cycle, no sensible acoustic pressure may develop. Therefore, the minimum flow velocity required for significant acoustic resonance depends on the particular acoustic radiation and other losses depending on the flow condition.

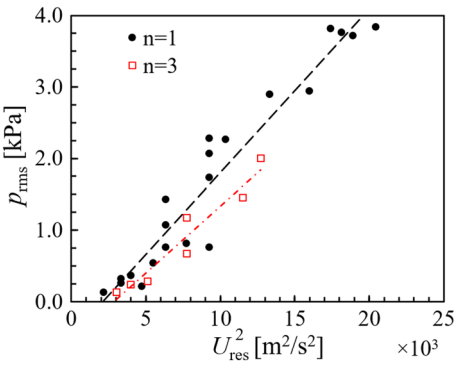



**Fig. 6** The acoustic pressure at the peak of acoustic resonance

The frequency dependence of the excited mode on the flow velocity at the peak of resonance is shown in Fig. 7. The data are scaled based on two different characteristic lengths, namely the cross section length and height. The figure shows that the excitation of the third mode conforms with a Strouhal number based on the cross section length, where $St_l$=0.49, which is similar to the Strouhal number of impinging leading-edge vortex instabilities (Nakamura et al. 1991). Such instabilities are sustained through a process wherein vortices are shed on blunt leading edges, convected downstream, then interact with the trailing edge, leading to a significant dependence on the streamwise characteristic length (Hourigan et al. 2001). This can explain the significant effect of the aspect ratio on the acoustic resonance excitation of the earlier resonance. Figure 7b suggests that the trailing-edge vortex shedding downstream of the cross section, which is characterized by $St_h = 0.11$, is responsible for the excitation of the first acoustic cross-mode.

An important trait of the acoustic resonance excitation is shown in Fig. 8. The wave number $k$ is the normalized acoustic frequency at the peak of acoustic resonance so that:

$$k = \frac{2\pi f}{c} \tag{2}$$

When adjusted for the mode number, Fig. 8 shows that the wave number decreases linearly as the acoustic resonance conditions occur at higher flow velocities. This decrease was observed for acoustic cross-modes in other configurations

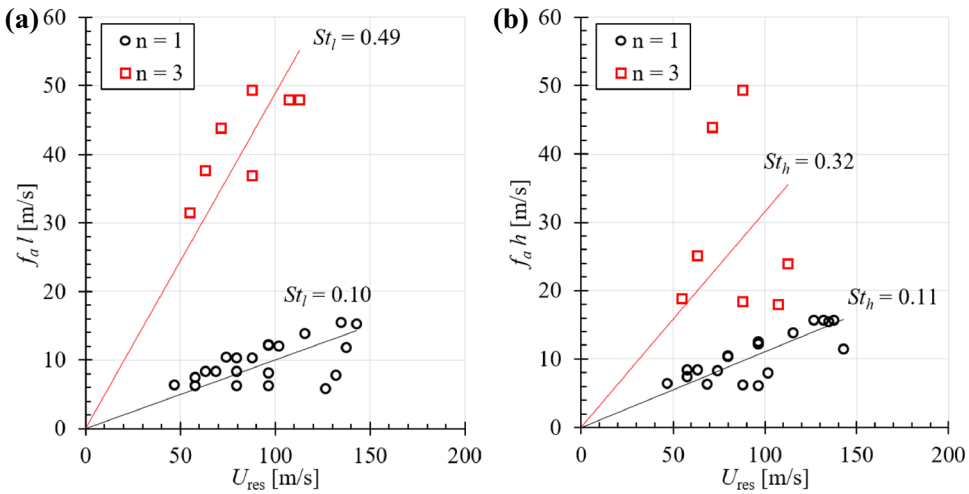



**Fig. 7** The Strouhal law of the first and third acoustic mode excitation based on the **a** Rod cross section length and **b** Rod cross section height

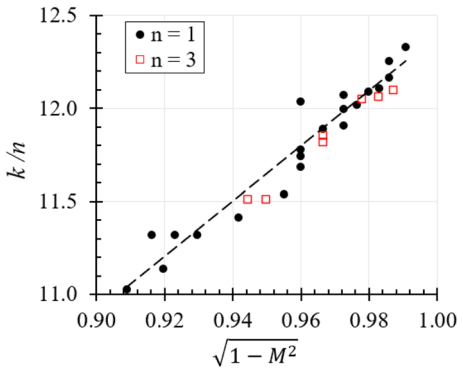



**Fig. 8** The acoustic resonance wave number dependency on the Mach number

such as uneven cylinders (Shaaban and Mohany 2019b), and therefore is characteristic of the acoustic mode regardless of the configuration which results in resonance excitation. As the flow velocity increases, acoustic resonance occurs at lower frequencies due to acoustic convective and added mass effects, similar to those in the case of vortex-induced vibration (Sarpkaya 2004). This steep decrease is vital to consider when estimating the coincidence condition, especially at higher Mach numbers.

## 4 Vortex dynamics in the wake during acoustic resonance

The excitation of acoustic resonance showed a significant dependency on the cross section dimensions of the rod, suggesting that the flow patterns in the wake play an important role in the resonance excitation mechanism. This section explores the main flow characteristics in the wake of four different configurations during acoustic resonance excitation. The periodic flow cycle is represented at eight phases, locked to the acoustic pressure phase $\varphi$. Figure 9 shows the vortex shedding pattern downstream of a rod with a square cross section at the peak of acoustic resonance excitation. For this cross section configuration with $h = l = 19.1$ mm, only the first acoustic cross-mode resonance was observed. At a flow velocity of $U_\infty = 96$ m/s, acoustic pressure had a tonal frequency $f_a = 638$ Hz representing the first acoustic mode at a root mean square pressure of $P_{\text{rms}} = 1729$ Pa. In Fig. 9, vorticity contours and streamlines are shown at eight phase-locked instants, with a step of 196 $\mu$s, starting at the instant of maximum acoustic particle velocity. The vortices are identified using the Lambda2 identifier (Jeong and Hussain 1995), plotted at a level of $\lambda 2 = -1$ in normalized terms. The alternative vortex shedding pattern in Fig. 9 shows that the interaction of the vortex with the side faces and the trailing corners results in a formation of a single vortex street. Although more elongated, this pattern has a significant similarity with shedding downstream of a circular cylinder.

The shedding patterns observed for a square cross section cylinder with $l = h = 25.4$ mm is shown in Fig. 10 at two different flow velocities representing the peak acoustic pressure at the two episodes of acoustic resonance. In Fig. 10a, the flow velocity $U_\infty = 88$ m/s resulted in the excitation of the third-mode acoustic resonance at $f_a = 1941$ Hz and $P_{\text{rms}} = 670$ Pa. At these conditions, vortices alternately interact with the trailing edges of the square cross section and then move downstream. The weakened shedding pattern further downstream in Fig. 10a suggests that the vortices at that region are not in complete sync with the acoustic pressure cycle, unlike the particular pattern on the two sides of the rod. This suggests that the excitation of acoustic resonances is driven by the interactions of the rod trailing edges with the shear layers separating from the leading corners. The Strouhal number based on the side length $l$ is $St_l = 0.55$, in agreement with typical values for shear layer instability.

In contrast, the first acoustic mode resonance is observed at $U_\infty = 134$ m/s for the same rod configuration. At its peak, the acoustic pressure reaches $P_{\text{rms}} = 3760$ Pa at a frequency of $f_a = 608$ Hz. The acoustic pattern shown in Fig. 10b clearly shows a single vortex street very similar to the pattern in Fig. 9 despite the significant increase in Reynolds number and the acoustic pressure, which indicates that the flow–acoustic coupling mechanism is similar in the two cases.

For a slender rod, the vortex patterns are vastly different during acoustic resonance excitation. Figure 11 presents phase-locked instants of the flow over the acoustic pressure cycle at the peak of resonance at two different conditions for a rod with $h = 12.7$ mm and $l = 25.4$ mm. Excitation of the first mode occurred at a flow velocity $U_\infty = 113$ m/s and reached $P_{\text{rms}} = 1729$ Pa. The interaction of the separated vortex shedding with the trailing edges resulted in an organized two-street shedding pattern. The Strouhal pattern at this condition, based on the side length $l$ is 0.42, still further away from the von-Karman vortex shedding and within typical values for shear layer instabilities. In the figure, the length of the cross section allows for the reattachment of the shear layer.

Looking at 11b, the flow pattern observed at the peak of the first-mode acoustic resonance is different than that in Fig. 11a despite the fact that the flow velocity is only 7% higher. At this condition, a flapping pattern can be seen for the two shear layers separating at the two sides of the rod, and the vortices are shed at a longer vortex formation length, although vorticity stays significant downstream. The cross section has the same dimensions and at nearly the same flow velocity, but the shear layer does not reattach on the sides of the rod. The higher length between vortices compared with the case in Fig. 11a is attributed to the frequency $f_a = 617$

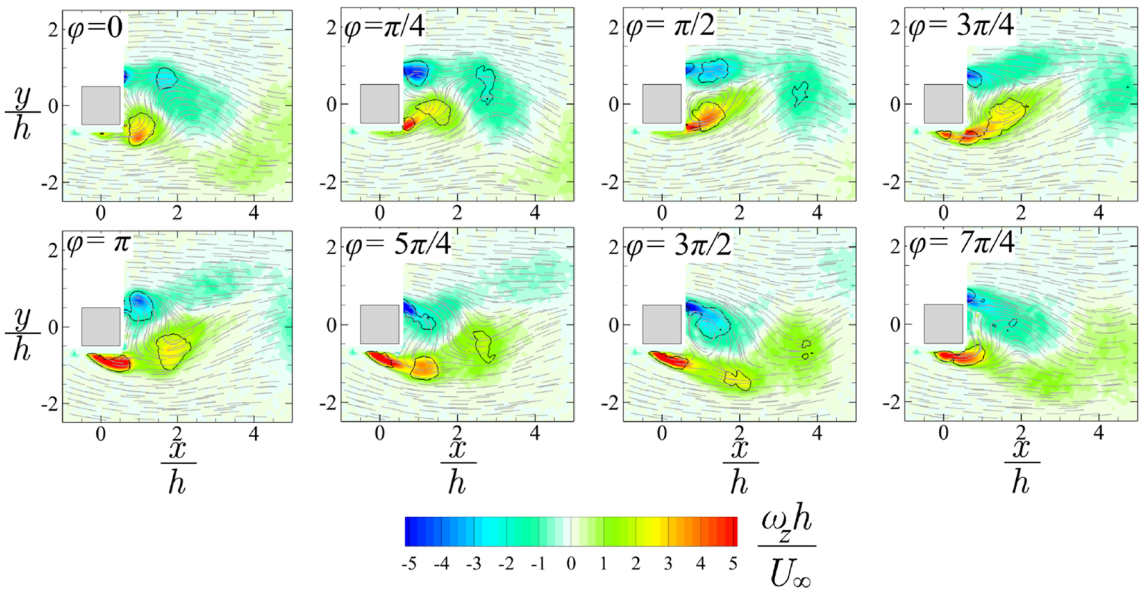



**Fig. 9** Flow characteristics in the wake of a rectangular rod with $l = 19.1$ mm and $h = 19.1$ mm over a cycle of acoustic resonance at its maximum acoustic pressure. Gray dashed streamlines and solid black $\lambda 2$ vortex indicators are superimposed on vorticity contours

Hz, about third its value for the other pattern, which means that the flow pattern needs to alternate much slower relative to the nearly unchanged flow velocity.

On the other hand, the vorticity shedding downstream of a block with side dimensions $h = 25.4$ mm and $l = 12.7$ mm is shown in Fig. 12 at the peak of the first mode resonance, with $U_\infty = 132$ m/s. The third mode was not excited for this configuration, while the first mode reached $P_{\text{rms}} = 3815$ Pa with a frequency of $f_a = 618$ Hz. Alternating vortex shedding resulting in a single vortex street is very organized downstream of this configuration, explaining the significantly higher acoustic resonance level, and the excitation of the first mode. The separating shear layers have minimal interaction with the trailing corners of the rod due to the short side length, which explains the minimal effect of $l$ on the Strouhal number for this aspect ratio. Moreover, the absence of the third acoustic mode resonance excitation can be attributed to the shorter side length $l$, which does not give rise to a shear layer instability between the leading and the trailing edges. From this discussion, one can associate certain periodic flow features to the excitation mechanism of the two different acoustic modes. The first mode acoustic resonance is excited by shedding pattern downstream of the rod. This pattern is characterized by a single street of vortices which can result in a higher acoustic resonance if vortices are more organized. The single frequency of vortex shedding increases linearly with the flow velocity, and therefore can excite the first acoustic mode at frequencies lower than the higher acoustic modes. The third acoustic mode excitation is associated with the interaction of the separating shear layers on the leading edge corners with the trailing edges of the rectangular configuration, an effect that is not possible for circular cylinders. For slender sections, this pattern leads to the formation of two parallel streets of alternating vortices. Shear layer instability occurs at multiple frequencies where the higher modes can occur at lower flow velocities (Xu et al. 2017), explaining why the third rather than the first mode is excited. Therefore, the first acoustic mode of the duct may be excited by a similar mechanism at substantially higher flow velocities, or smaller rod sections. Due to the higher Strouhal numbers of shear layer instability, the flow velocity at which the first mode excitation is expected is much higher than that of the vortex shedding mechanism for a square cross section. However, the flow velocities at which resonance is excited by the two different mechanisms are independent and can be obtained by consideration of the Strouhal number, Reynolds number, and the dimensions of the rod cross section and the rectangular duct.

## 5 Effect of the flow incidence angle on the resonance excitation mechanism

Results discussed in the previous sections showed that the aeroacoustic response of square cylinders is dependent on the flow regime around the rod cross section. Therefore, the flow incidence angle is an important parameter to consider due to its $Re$ = significant impact on the flow regimes in the wake. Two different cross sections are used to identify the effect of the Reynolds number on the excitation of acoustic resonance. For an edge length $l = 19.1$ mm, measurements were carried out between $Re = 1.2\times10^4$ and $1.0\times10^5$, and

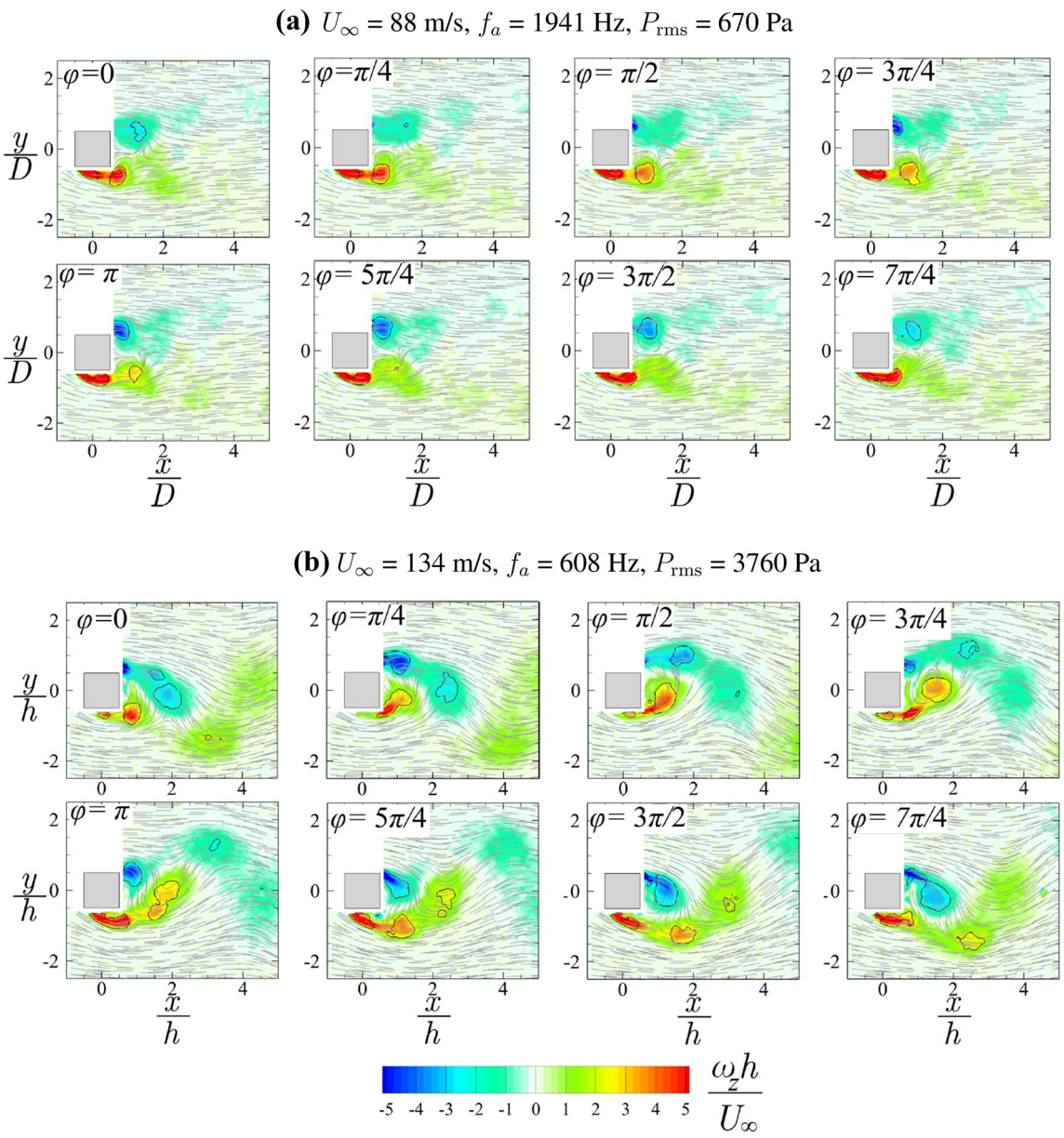



**Fig. 10** Flow characteristics in the wake of a rectangular rod with $l$ = 25.4 mm and $h$ = 25.4 mm over a cycle of acoustic resonance at its maximum acoustic pressure. Gray dashed streamlines and solid black $\lambda 2$ vortex indicators are superimposed on vorticity contours

for an edge length $l$ = 25.4 mm, the Reynolds number range was $1.6\times10^4$ to $1.3\times10^5$. The incidence angle was varied between 0° and 45°, with a step of 9°, covering the range of possible configurations due to the rod symmetry. For rods attached at any flow incidence angle $\alpha$, resonance excitation of the first acoustic cross-mode of the duct was observed at the coincidence of a vortex shedding peak in the acoustic pressure spectra, with the acoustic mode frequency. However, the incidence angle $\alpha$ had a significant effect on the characteristics of the acoustic resonance excitation. As the incidence angle $\alpha$ increases from 0° to 45°, the flow can have different flow regimes according to the Reynolds numbers, the asymmetry, the formation of side bubbles, and the reattachment on the trailing faces (Norberg 1993). In the next discussion, the Strouhal number and the acoustic pressure during resonance excitation is discussed, and a summary of the results is presented.

Figure 13 shows the effect of the incidence angle on the Strouhal number at the peak of the first acoustic mode resonance based on the edge length $l$. Measurements agree well with the results of Yen and Yang (2011). In the range of 0° to 15°, the Strouhal number increases to a peak, then drops again until its value at 45° is lower than 0.125. Notably, the

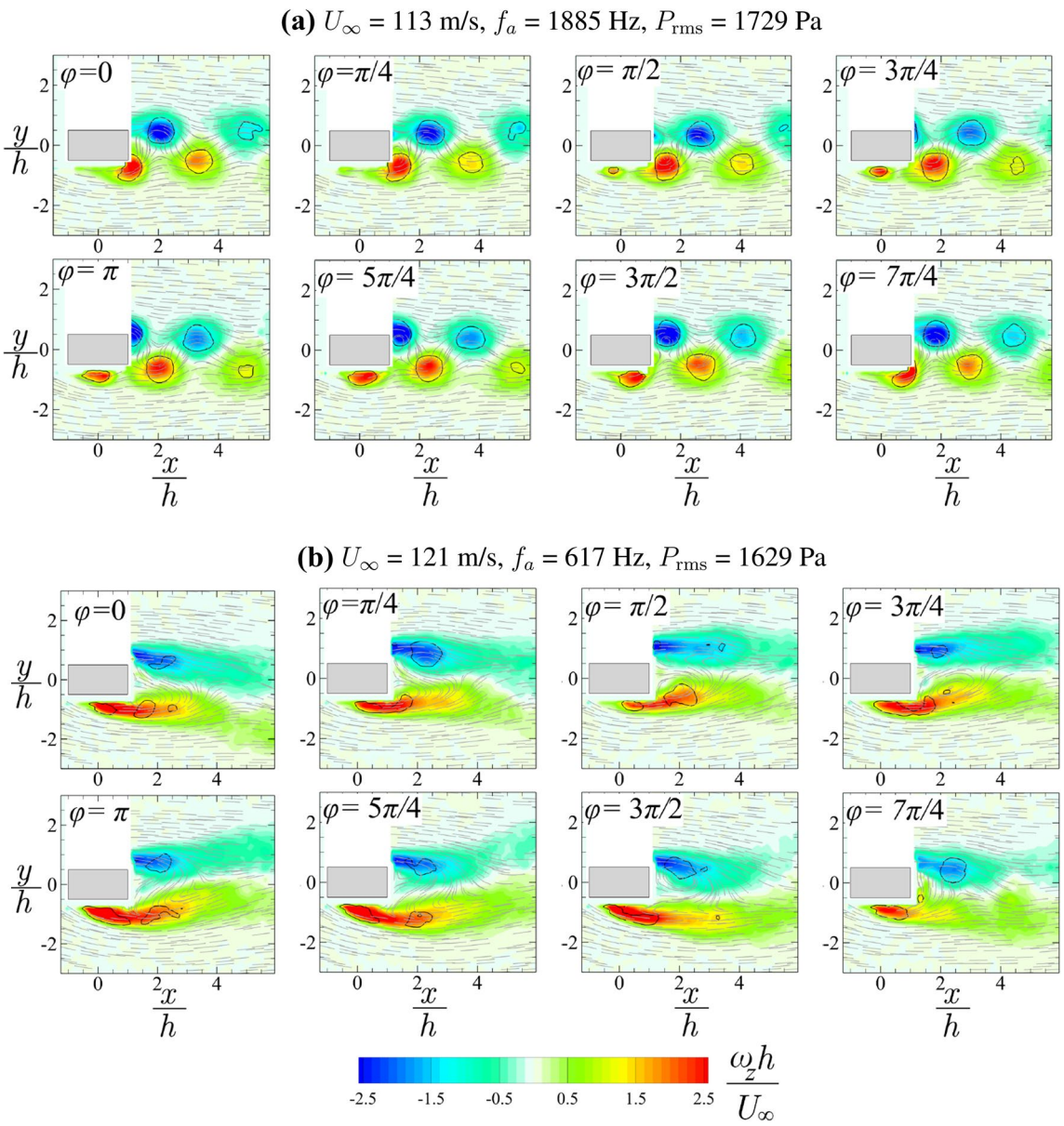



**Fig. 11** Flow characteristics in the wake of a rectangular rod with $l$ = 25.4 mm and $h$ = 12.7 mm over a cycle of acoustic resonance at its maximum acoustic pressure. Gray dashed streamlines and solid black $\lambda 2$ vortex indicators are superimposed on vorticity contours

Strouhal number has no dependence on Reynolds number at angles of attack lower than 15°, but a slight dependence is visible at higher incidence angles.

Figure 14 shows the effect of the angle of attack on the Strouhal number $St_d$ based on the blockage length $d = l(\sin\alpha + \cos\alpha)$, which was shown by Knisely (1990) to have a strong effect on the flow around rods of rectangular cross sections. Figure 14 shows that the Strouhal numbers responsible for resonance excitation are in good agreement with the values reported in the literature for the periodic patterns of vortex shedding downstream of the rod. Therefore, the general pattern of flow that is able to couple with the acoustic field and excite resonance shares the characteristics identified in the literature for this range of incidence angle. At incidence angles of 0°, the separated flow reattaches on the side of the rod before separating again from the trailing corners, and therefore, the angle of incidence has a significant effect on the Strouhal number, increasing from 0.135 to 0.19. At incidence angles higher than 15°, the Strouhal number is stable at about 0.17 as the flow regime is fully separated and no reattachment of the shear layer on the sides is observed. This significant effect is expected to influence the mechanism of acoustic resonance excitation.

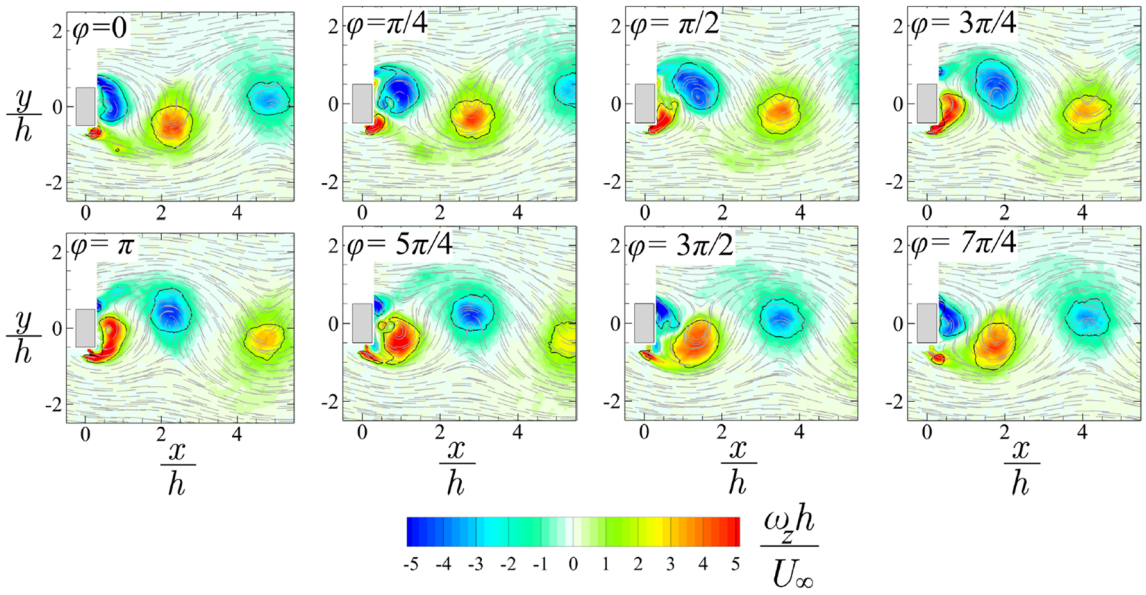



**Fig. 12** Flow characteristics in the wake of a rectangular rod with $l = 12.7$ mm and $h = 25.4$ mm over a cycle of acoustic resonance at its maximum acoustic pressure. Gray dashed streamlines and solid black $\lambda 2$ vortex indicators are superimposed on vorticity contours

Figure 15 shows the effect of the incidence angle on the range of flow velocities during lock-in $\Delta U_{res} = U_{max} - U_{min}$, over which the normalized acoustic pressure is elevated. The maximum acoustic pressure occurs at $U_{res}$. The figure clearly shows that the pattern of flow has an effect on the lock-in range that depends on the excited mode and the edge length $l$. For the two configurations where vortex shedding is symmetric at $\alpha = 0°$ and $\alpha = 45°$, the effect of the side length on the normalized lock-in flow velocity range is minimal. On the other hand, acoustic resonance and lock-in are observed over a significantly wider range of flow velocities for the larger cross section at incidence angles higher than 15°.

Figure 16 shows the effect of the incidence angle on the acoustic pressure at the peak of resonance for rods with two different edge lengths. The value of acoustic pressure is normalized by the inlet kinetic energy 1/2 $\rho U_{res}^2$, where $U_{res}$ is the flow velocity at the peak of acoustic resonance. Results suggest that the incidence angle has a significant effect on the excitation mechanism. First, the third mode excitation is only

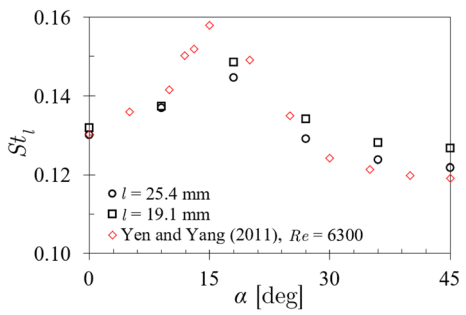



**Fig. 13** The effect of the incidence angle $\alpha$ on the Strouhal number at the peak of the first acoustic mode resonance, based on the side length $l$

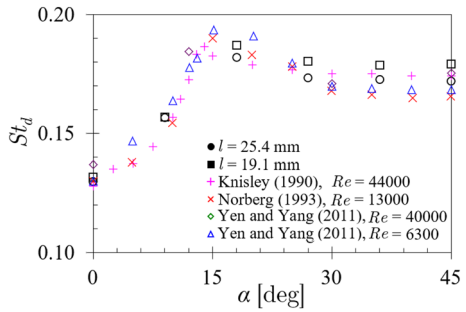



**Fig. 14** The effect of the incidence angle $\alpha$ on the Strouhal number based on the blockage length $d$

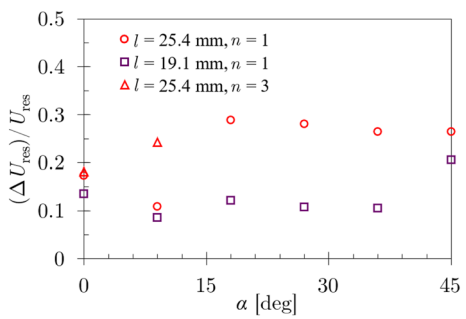



**Fig. 15** The effect of incidence angle on the lock-in flow velocity range

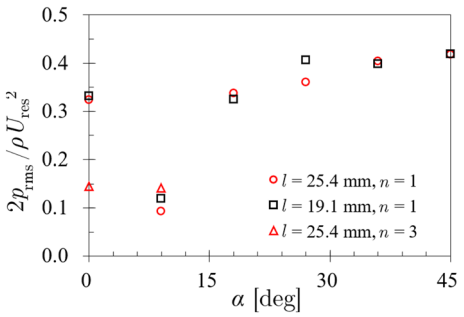



**Fig. 16** The normalized acoustic pressure dependency on the incidence angle at the peak of resonance

observed at low incidence angle for the rod with a larger side length. This can be explained by the change in the flow pattern at higher incidence angles, where the symmetric separation of the shear layers and their interaction with the trailing edges is not possible. As $\alpha$ approaches 45°, the shear layer separation mainly occurs at the two opposite corners of the symmetric diamond cross section that points in the flow direction. Second, the normalized acoustic pressure has no dependency on the block size, which is an indication that the acoustic pressure scales with $U^2$ similar to the case of a single rectangular cavity (Aly and Ziada 2016; Shaaban and Mohany 2015). The two situations share the similar attribute that separation occurs at a fixed location regardless of the Mach number and flow regime, unlike circular cylinders. Moreover, the excitation of acoustic resonance is maximum at an incidence angle of 45°, suggesting that the symmetry of vortex shedding plays an important role in resonance excitation. Similar to the Strouhal numbers, the excitation of acoustic resonance is sensitive to the incidence angle for $0° \leq \alpha \leq 15°$, while there is a slight increase at higher incidence angles.

From this discussion, it becomes clear that the symmetry of the vortex shedding pattern plays an important role in the mechanism of acoustic resonance excitation for rods with square cross sections. The sensitivity of Strouhal numbers to the incidence angle means that careful consideration of its effects on the resonance parameters is important to avoid the excitation of acoustic resonance. Although asymmetric vortex shedding seems to alleviate the intensity of acoustic resonance, it occurs at lower flow velocities which may impose a limit on operating conditions. Moreover, cross sections at low incidence angles impose a wider lock-in range and may also result in the excitation of the third mode.

## 6 Conclusion

Oscillating flow patterns in the wake of a rectangular rod with sharp edges were able to couple with the acoustic modes of the duct and excite strong acoustic resonance. Unlike circular cylinders, the acoustic resonance of the third acoustic transverse mode was excited by lower flow velocities than required for coincidence between the frequencies of the vortex shedding and the acoustic mode. Vortex shedding downstream of the rod is able to excite the first acoustic cross-mode for all aspect ratios *l*/*h*. Resonance is excited at the coincidence of the first acoustic mode frequency with the vortex shedding frequency, characterized by the Strouhal number which has a significant dependency on the aspect ratio. Second, the interaction of the shear layers separating at the leading edges with the trailing edges coupled with the third acoustic cross-mode of the duct in some cases with larger side length. This excitation was characterized by a higher Strouhal number that depends on the side length of the rod. The pressure level at the peak of acoustic resonance excitation is proportional to the incoming flow kinetic energy. The flow incidence angle affects the excitation of acoustic resonance significantly for square cross sections. The acoustic pressure and the lock-in range are sensitive to low incidence angles, but stable for higher incidence angles. The characteristic Strouhal number for resonance excitation had a strong dependence on the flow regime around the blocks, although not significantly dependent on Reynolds number.

**Acknowledgements** The authors would like to acknowledge the financial support provided by the Natural Sciences and Engineering Research Council of Canada (NSERC).

## Declarations

**Conflict of interest** The authors declare that they have no conflict of interest.

## References

Aly K, Ziada S (2016) Review of flow-excited resonance of acoustic trapped modes in ducted shallow cavities. J Pressure Vessel Technol 138(4):216

Bearman P, Trueman D (1972) An investigation of the flow around rectangular cylinders. Aeronaut Q 23(3):229–237

Bearman P, Gartshore I, Maull D, Parkinson G (1987) Experiments on flow-induced vibration of a square-section cylinder. J Fluids Struct 1(1):19–34

Blevins R (1984) Review of sound induced by vortex shedding from cylinders. J Sound Vibr 92(4):455–470

Blevins R (1985) The effect of sound on vortex shedding from cylinders. J Fluid Mech 161:217–237

Blevins R, Bressler M (1993) Experiments on acoustic resonance in heat exchanger tube bundles. J Sound Vibr 164(3):503–533

Brooks PNH (1960) Experimental investigation of the aeroelastic instability of bluff two-dimensional cylinders. PhD thesis, University of British Columbia

Clark ST, Besem FM, Kielb RE, Thomas JP (2015) Developing a reduced-order model of nonsynchronous vibration in

turbomachinery using proper-orthogonal decomposition methods. J Eng Gas Turbines Power 137(5):871
da Silva Pinto WJG, Margnat F (2020) Shape optimization for the noise induced by the flow over compact bluff bodies. Computers & Fluids 198:104400
Dequand S, Hulshoff S, Hirschberg A (2003) Self-sustained oscillations in a closed side branch system. J Sound Vibr 265(2):359–386
Dobre A, Hangan H (2004) Investigation of the three-dimensional intermediate wake topology for a square cylinder at high reynolds number. Exper Fluids 37(4):518–530
Dutta S, Muralidhar K, Panigrahi P (2003) Influence of the orientation of a square cylinder on the wake properties. Exper Fluids 34(1):16–23
Fiquet AL, Vercoutter A, Buffaz N, Aubert S, Brandstetter C (2020) Acoustic resonance in an axial multistage compressor leading to non-synchronous blade vibration. In: ASME Turbo Expo 2020: Turbomachinery Technical Conference and Exposition, American Society of Mechanical Engineers Digital Collection
Hourigan K, Thompson MC, Tan BT (2001) Self-sustained oscillations in flows around long blunt plates. J Fluids Struct 15(3–4):387–398
Inoue O, Hatakeyama N (2002) Sound generation by a two-dimensional circular cylinder in a uniform flow. J Fluid Mech 471:285–314
Islam MR, Shaaban M, Mohany A (2020) Vortex dynamics and acoustic sources in the wake of finned cylinders during resonance excitation. Phys Fluids 32(7):075117
Jeong J, Hussain F (1995) On the identification of a vortex. J Fluid Mech 285:69–94
Keller J, Escudier M (1983) Flow-excited resonances in covered cavities. J Sound Vibr 86(2):199–226
Knisely CW (1990) Strouhal numbers of rectangular cylinders at incidence: a review and new data. J Fluids Struct 4(4):371–393
Léon O, Méry F, Piot E, Conte C (2019) Near-wall aerodynamic response of an acoustic liner to harmonic excitation with grazing flow. Exper Fluids 60(9):1–18
Mancinelli M, Jaunet V, Jordan P, Towne A (2019) Screech-tone prediction using upstream-travelling jet modes. Exper Fluids 60(1):22
Margnat F (2015) Hybrid prediction of the aerodynamic noise radiated by a rectangular cylinder at incidence. Computers & Fluids 109:13–26
Mohany A, Ziada S (2005) Flow-excited acoustic resonance of two tandem cylinders in cross-flow. J Fluids Struct 21(1):103–119
Mohany A, Ziada S (2011) Measurements of the dynamic lift force acting on a circular cylinder in cross-flow and exposed to acoustic resonance. J Fluids Struct 27(8):1149–1164
Nakamura Y, Ohya Y, Tsuruta H (1991) Experiments on vortex shedding from flat plates with square leading and trailing edges. J Fluid Mech 222:437–447
Norberg C (1993) Flow around rectangular cylinders: pressure forces and wake frequencies. J Wind Eng Industrial Aerodyn 49(1–3):187–196
Norberg C (2003) Fluctuating lift on a circular cylinder: review and new measurements. J Fluids Struct 17(1):57–96
NRC (2004) Additional flow-induced vibration failures after a recent power uprate. NRC Inf Notice 2002–26(Supplement):2
Okajima A (1982) Strouhal numbers of rectangular cylinders. J Fluid Mech 123:379–398
Parker R, Welsh M (1983) Effects of sound on flow separation from blunt flat plates. Int J Heat Fluid Flow 4(2):113–127
Pereira LTL, Ragni D, Avallone F, Scarano F (2020) Pressure fluctuations from large-scale piv over a serrated trailing edge. Exper Fluids 61(3):1–17
Rockwell D, Naudascher E (1978) Self-sustaining oscillations of flow past cavities. J Fluids Eng 100(2):152–165
Rockwell DO (1977) Organized Fluctuations Due to Flow Past a Square Cross Section Cylinder. J Fluids Eng 99(3):511–516
Sarpkaya T (2004) A critical review of the intrinsic nature of vortex-induced vibrations. J Fluids Struct 19(4):389–447
Sciacchitano A, Wieneke B (2016) Piv uncertainty propagation. Measure Sci Technol 27(8):084006
Shaaban M, Mohany A (2015) Passive control of flow-excited acoustic resonance in rectangular cavities using upstream mounted blocks. Exper Fluids 56(4):72
Shaaban M, Mohany A (2019) Characteristics of acoustic resonance excitation by flow around inline cylinders. J Pressure Vessel Technol 141(5):971
Shaaban M, Mohany A (2019) Phase-resolved piv measurements of flow over three unevenly spaced cylinders and its coupling with acoustic resonance. Exper Fluids 60(4):71
Shaaban M, Mohany A (2020) Experimental study of the self-excited resonance effect on the dynamic lift and flow structure around inline cylinders. J Fluids Struct 96:68
Tian J, Yao D, Wu Y, Ouyang H (2018) Experimental study on rotating instability mode characteristics of axial compressor tip flow. Exper Fluids 59(4):1–13
Tonon D, Hirschberg A, Golliard J, Ziada S (2011) Aeroacoustics of pipe systems with closed branches. Int J Aeroacoust 10(2–3):201–275
Uchiyama Y, Morita R (2017) Flow-induced acoustic resonance in a closed side branch under a low-pressure wet steam flow. J Pressure Vessel Technol 139(3):871
Van Oudheusden B, Scarano F, Van Hinsberg N, Watt D (2005) Phase-resolved characterization of vortex shedding in the near wake of a square-section cylinder at incidence. Exper Fluids 39(1):86–98
van Hinsberg NP (2021) Aerodynamics of smooth and rough square-section prisms at incidence in very high reynolds-number cross-flows. Exper Fluids 62(3):1–17
Welch P (1967) The use of fast fourier transform for the estimation of power spectra: a method based on time averaging over short, modified periodograms. IEEE Trans Audio Electroacoust 15(2):70–73
Xu J, Lei J, Wu J, Zhang K (2017) The three-dimensional characteristics of the unsteady wall-pressure in a low-mach-number rectangular cavity flow with rossiter model oscillation. Exper Fluids 58(9):1–15
Yen SC, Yang CW (2011) Flow patterns and vortex shedding behavior behind a square cylinder. J Wind Eng Industr Aerodyn 99(8):868–878
Zhang P, Wang J, Lu S, Mi J (2005) Aerodynamic characteristics of a square cylinder with a rod in a staggered arrangement. Exper Fluids 38(4):494–502
Ziada S (2010) Flow-excited acoustic resonance in industry. J Pressure Vessel Technol 132(1):015001
Ziada S, Shine S (1999) Strouhal numbers of flow-excited acoustic resonance of closed side branches. J Fluids Struct 13(1):127–142
Ziada S, Oengören A, Bühlmann E (1989) On acoustical resonance in tube arrays part i: Experiments. J Fluids Struct 3(3):293–314

**Publisher's Note** Springer Nature remains neutral with regard to jurisdictional claims in published maps and institutional affiliations.